

Study on the fabrication of active CaO from steel slag of the converter and its application in CO₂ adsorption process

J. Cheng ^a, R. Mao ^{a,b}, F. Wang ^a, H.-W. Yao ^a, Z.-b. Yang ^c

^a Jiangsu (Shagang) Iron and Steel Research Institute, Zhangjiagang, China;

^b Jiangsu Shagang Group Co. LTD, Zhangjiagang, China;

^c School of Jiangsu University of Science and Technology, Metallurgical Engineering, Zhangjiagang, China

Jie Cheng: chengjie-iris@shasteel.cn; Rui Mao: maorui0138@163.com;

Fei Wang: wangfei-iris@shasteel.cn; Haiwei Yao: yaohw-iris@shasteel.cn;

Zhibin Yang: zhibinyang@shu.edu.cn

(Received 25 October 2024; Accepted 09 May 2025)

Abstract : An acetic acid leaching process was employed to extract calcium components from converter steel slag, followed by evaporation and crystallization to obtain high-purity CaO material. The effects of various leaching parameters on the CaO content were systematically investigated. The shrinking core model was used to analyze the leaching rate of weakly acidic solutions. Subsequently, the CO₂ adsorption performance of the CaO material under different conditions was evaluated, and the adsorption process and reaction mechanism were examined using XRD and SEM analysis. Results indicated that leaching temperature and acetic acid concentration significantly influenced the CaO content. Optimal leaching parameters were determined to be an acid concentration of 1 M, a solid-to-liquid ratio of 1:10, a leaching temperature of 70 °C, and a duration of 2 h, achieving a maximum CaO content of 86.3%. Kinetic studies revealed that stirring shifted the rate-controlling step of calcium leaching from external diffusion and surface chemical reactions to internal diffusion. Within the temperature range of 40-70 °C, internal diffusion governed the rate-controlling step. XRD and SEM analyses confirmed the high purity of the CaO material. CaO initially transformed into Ca(OH)₂, which adsorbed CO₂ to form CaCO₃. The deposition of CaCO₃ on the material surface hindered further contact between Ca(OH)₂ and CO₂, reducing carbon adsorption efficiency and increasing the CaO content, markedly enhanced adsorption performance. In the adsorption temperature range of 0-100 °C, ensuring effective contact between Ca(OH)₂ and CO₂ was critical. The calculated CO₂ capture capacities at 30 °C, 50 °C, and 70 °C were 0.32 g/g, 0.24 g/g, and 0.17 g/g, respectively. This study provides valuable insights into the high-value utilization of steel slag and the reduction of CO₂ emissions in iron and steel enterprises.

Keyword : Steel slag; CO₂ emission reduction; Calcium-based adsorbent; Metal element recovery; Acid leaching kinetics

In China, nearly 100 Mt/a of steel slag is generated annually, most accumulating without being effectively utilized. Due to the presence of free calcium oxide in steel slag, it reacts with rainwater to form Ca(OH)₂, which seeps into the ground, causing soil pH imbalance and environmental harm [1]. In some regions of Japan and Europe, the utilization rate of steel slag approaches 100%. However, only 22% of the annually produced steel slag is utilized in China [2], a significantly lower rate. Therefore, various industrial methods have been proposed to enhance the resource utilization of steel slag, among which steel slag carbonation is an effective strategy. In carbonating steel slag, CO₂ can be sequestered, thus achieving the dual goal of reducing CO₂ emissions.

Due to its large output and high calcium content, steel slag is a promising material for carbon adsorption. However, since calcium in steel slag primarily exists in the stable form of calcium silicate phases, its direct use for CO₂ capture is less effective. Consequently, research on leaching, extracting,

and recovering calcium from steel slag for subsequent CO₂ capture has garnered significant attention [3-6]. Selective leaching agents are widely employed to extract valuable components from steel slag. Studies on the extraction of active ingredients using water or ammonium salt leaching have been extensively conducted [7-9]. Given the presence of CaO in steel slag, acid treatment can also readily leach calcium, thereby increasing the concentration of essential elements in the leachate. Y. H. Lee found that acetic acid can effectively leach calcium from steel slag, and the smaller the particle size, the faster the Ca²⁺ leaching rate [10]. The increase in Ca²⁺ concentration in the leachate enhances CO₂ absorption. However, unreacted acid in the leachate lowers the solution's pH, hindering direct carbonation. In contrast, solid calcium-based materials prepared from steel slag exhibit significantly improved CO₂ capture capacity. L.L Li used acetic acid to extract Ca²⁺, then added NaCO₃ solution to precipitate and prepare calcium-based materials [11]. The results showed CO₂ adsorption capacities of 30.8 mg/g for pure CO₂ gas and 19.1 mg/g for blast furnace gas.

Steel slag is a complex solid waste rich in metal elements such as Fe, Si, Mg, and Al. Using precipitants increases process costs and reduces the material's purity. In fact, due to the complex mineral composition and the presence of various metal elements, the acid-leaching process of steel slag becomes intricate and multifaceted. Different leaching conditions influence the chemical composition of the subsequently prepared adsorbents, affecting their carbon capture performance [12,13]. Presently, research on the leaching treatment of steel slag primarily focuses on extracting Ca²⁺, while studies on converting Ca²⁺ into solid, active CaO materials remain relatively scarce.

Moreover, understanding the leaching mechanism of calcium from steel slag is crucial for achieving an efficient carbonation process. In the steel industry, numerous studies have explored the dissolution mechanism of calcium in steel slag. Some researchers have conducted kinetic analyses of calcium leaching from slag into water using kinetic models to elucidate the leaching mechanism precisely [14-16]. Yokoyama demonstrated that the leaching of calcium from slag is controlled by diffusion through the surface layer [17], while Kashiwaya [15] reported that as particle size increases, the rate-controlling step of calcium leaching changes. However, these kinetic studies were not conducted under acidic conditions, as calcium tends not to precipitate in such environments. Nevertheless, studying the kinetics of calcium leaching under acidic conditions is essential.

This study treated converter steel slag using a weak acid leaching-evaporation crystallization method to obtain CO₂ adsorbent materials with high CaO content. The effects of acid concentration, solid-liquid ratio, temperature, and leaching time on the CaO content of the material were investigated, and the leaching kinetics of calcium in a weak acid environment were analyzed. CO₂ adsorption experiments were conducted on the prepared CaO materials, examining the influence of CaO content, CO₂ concentration, and adsorption temperature on adsorption performance. Additionally, the adsorption process and reaction mechanisms were explored.

1. Experimental Section

1.1 Materials and Reagents

In this study, a steel plant in Jiangsu supplied the converter steel slag. After grinding, sieving, and drying, three particle size fractions were selected for the experiments: (i) <100 μm, (ii) 100-500 μm, and (iii) 500-1000 μm. The CaO content of the steel slag was measured using a ZSX Primus II X-ray fluorescence spectrometer, yielding a result of 36.6 wt%. Furthermore, X-ray diffraction (XRD) analysis was conducted on the steel slag samples, revealing the main phases to be dicalcium silicate (C₂S), tricalcium silicate (C₃S), dicalcium ferrite (C₂F), and the RO phase (CaO-FeO-MnO-MgO solid solution), along with free calcium oxide (f-CaO) (See Fig.1). All reagents used in the experiments were of analytical grade, including acetic acid (C₂H₄O₂, AR, ≥99.5 wt%, Shanghai Pharmaceutical Group Chemical Reagent Co., Ltd.) and deionized water. Zhangjiagang Southeast Gas Filling Co., Ltd provided the experimental gases utilized in this study.

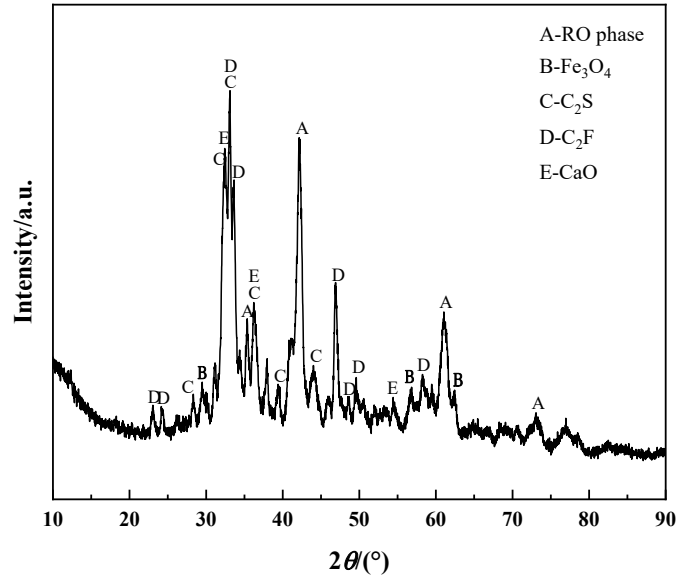


Fig.1 XRD pattern of the steel slag

1.2 Synthesis of CaO materials

First, the acetic acid solution was diluted to a specific concentration. Then, in a separable flask, the steel slag samples were mixed with the corresponding concentration of acetic acid solution at a set solid-to-liquid ratio. A magnetic stirrer is used to stir the mixture continuously at a controlled temperature, maintaining a stirring rate of approximately 600 rpm (Fig 2, Step 1). After reaching the predetermined reaction time, stirring was stopped, and the mixture was subjected to centrifugation (Step 2) to obtain the steel slag leachate and the centrifuged precipitate (i.e., the acid leaching residue). The leachate was dried at 105 °C for 12 h (Step 3). The dried material was then calcined at 900 °C in a muffle furnace for 2 h (Step 4) to synthesize the CaO material.

Investigate the effects of operational parameters such as initial acid concentration (L1), solid-to-liquid ratio (L2), leaching temperature (L3), and leaching time (L4) on the CaO content in the material, four sets of single-factor experiments were designed, as shown in Table 1. Additionally, the experiments explored the relationship between Ca^{2+} leaching rate and time at different stirring rates and temperatures to study the kinetics of calcium leaching reactions. During leaching, 1 ml samples were periodically extracted and filtered using a membrane filter with a pore size of 0.8 μm . Subsequently, the concentration of Ca^{2+} in the samples was measured using ICP-OES, and the leaching rate was calculated. The calculation formula is as follows:

$$L_{Ca} = \frac{C_i V}{m W_i} \times 100\% \quad (1)$$

Here: $L_{Ca}(\%)$ is the leaching rate of Ca^{2+} , $m(\text{g})$ is the initial mass of the steel, $W_i(\%)$ is the mass fraction of CaO in the chemical composition of the steel slag, $C_i(\text{mg/l})$ is the concentration of Ca^{2+} in the leachate, $V(\text{ml})$ is the volume of the leachate.

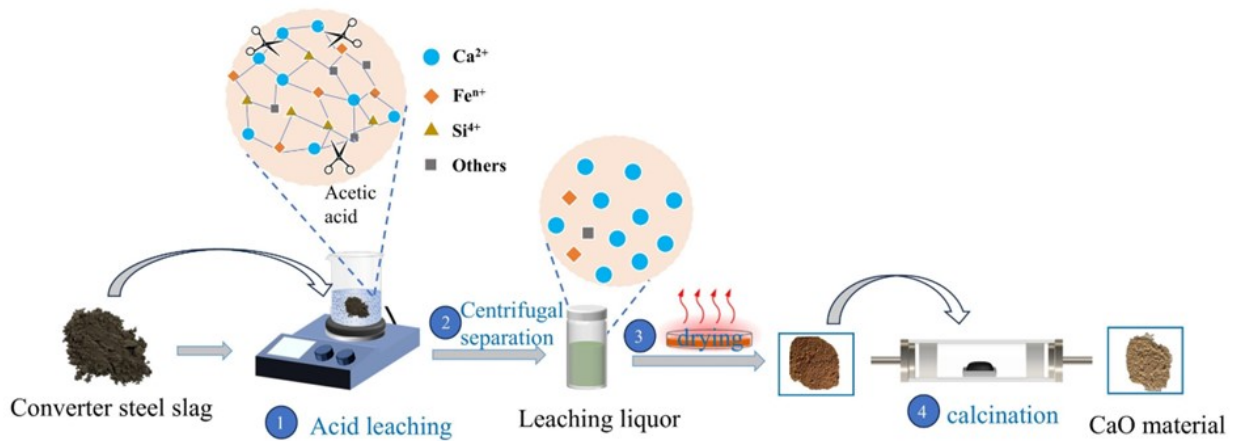


Fig.2 Schematic Illustration of the Synthetic Procedure for the Preparation of the CaO material from Converter Steel Slag

Table 1 Single-factor experimental parameters of the acetic acid leaching process

Other parameters	L1 /M	Other parameters	L2/g: ml	Other parameters	L3/°C	Other parameters	L4 /h
	1		1:10		30		0.5
L2: 1:25	2	L1: 2/M	1:15	L1: 2/M	40	L1: 2/M	1
L3: 70/°C	3	L3: 70/°C	1:20	L2: 1:10	50	L2: 1:10	1.5
L4: 2/h	4	L4: 2/h	1:25	L4: 2/h	60	L3: 70/°C	2
	5		1:30		70		2.5

1.3 CO₂ adsorption

A specified mass of CaO material was placed in a sealed container, and the programmed temperature was set while a mixed gas of CO₂ and water vapor was introduced. The gas flow was monitored using a flow display control instrument, initially set to 1 L/min. The adsorption process lasted for 2 h. After adsorption, a sample of a certain mass was extracted and placed in an alumina crucible. Subsequently, the crucible was placed in a synchronous thermogravimetric analyzer for the desorption reaction. The temperature was programmed to rise to 1000 °C at a heating rate of 15 °C/min. Throughout the heating process, weight loss was monitored, and the characteristic peaks of CO₂ desorption were recorded to assess the CO₂ adsorption performance.

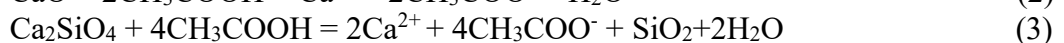
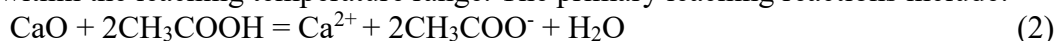
1.4 Characterization Methods

The elemental composition and content of the CaO material were determined using a ZSX Primus II X-ray fluorescence spectrometer. The crystallographic phases of the CaO material before and after CO₂ adsorption were characterized using an Ultima IV X-ray diffractometer. Additionally, a JSM-6510LA scanning electron microscope was employed to observe the structural and surface morphology of the CaO material before and after CO₂ adsorption.

2. Results and Discussion

2.1 Thermodynamics of Leaching

The thermodynamics of the acid-leaching reactions of calcium-containing phases in steel slag were calculated within the leaching temperature range. The primary leaching reactions include:



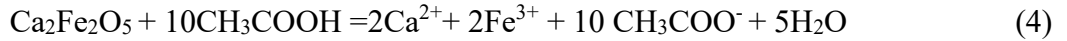


Fig.3 illustrates the variation in Gibbs free energy (ΔG) for calcium leaching reactions at different temperatures. Within the range of 0-100 °C, the ΔG of the reactions between CaO and Ca_2SiO_4 in steel slag with CH_3COOH is less than 0, indicating a strong thermodynamic tendency for these minerals to react spontaneously with CH_3COOH under atmospheric pressure. In contrast, the ΔG for the reaction between $\text{Ca}_2\text{Fe}_2\text{O}_5$ and CH_3COOH is negative within the 0-50 °C range but gradually becomes positive as the temperature increases, suggesting that the reaction is somewhat hindered at higher temperatures. Moreover, at lower temperatures, the reaction tendency of $\text{Ca}_2\text{Fe}_2\text{O}_5$ with CH_3COOH is weaker compared to that of Ca_2SiO_4 and CaO, indicating that the reactivity of $\text{Ca}_2\text{Fe}_2\text{O}_5$ is influenced by temperature and the reaction medium, exhibiting distinct characteristics in comparison to the other compounds.

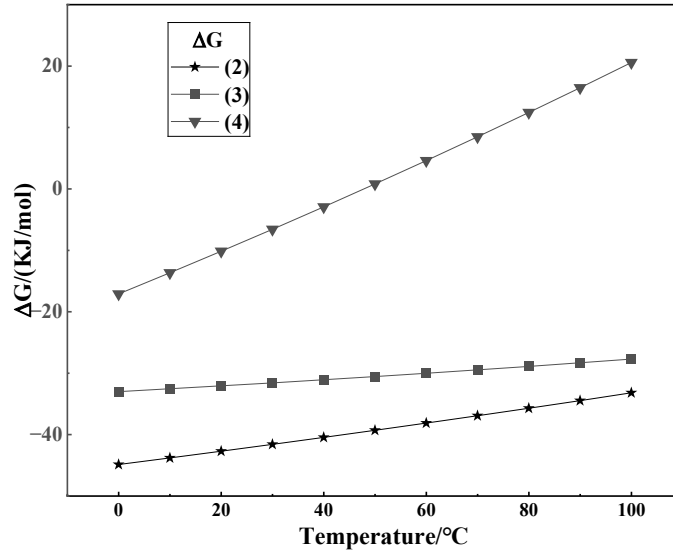


Fig.3 Gibbs free energy of acid hydrolysis reaction of main calcium-base phase in steel slag at different temperatures (atmospheric pressure)

2.2 Influence of leaching parameters on CaO content of materials

2.2.1 Initial acid concentration

As shown in Fig.4a, the variation in acid concentration and particle size leads to significant differences in the mass fraction of CaO. As the acid concentration increases, the CaO content exhibits a decreasing trend. At a concentration of 1 M, the CaO content reaches its peak at 82.7%. This phenomenon is due to the increase in acetic acid concentration, and the H^+ concentration also rises, making the mineral phases on the surface of the steel slag more accessible, thereby enhancing the probability and rate of reaction. Although the leaching of calcium increases, the leaching of other elements from the steel slag also intensifies, resulting in a reduction in the CaO content in the material. Additionally, the CaO content increases with the particle size of the steel slag, which may be attributed to the significant differences in Ca element content among steel slag samples of varying particle sizes. In conclusion, the concentration of acetic acid has a pronounced effect on CaO content, with low concentrations of acetic acid effectively increasing the CaO content.

2.2.2 Solid-liquid ratio

As shown in Fig.4b, with the increase in the solid-to-liquid ratio, the CaO mass fraction initially decreases, then rises, followed by another decline. At a solid-to-liquid ratio of 1:10, the CaO content reaches its highest point at 86.3%. The initial decrease can be attributed to the increase in the solid-to-liquid ratio, which also increases the content of other elements in the material. Similarly, when the solid-to-liquid ratio is low, the H^+ content in the solution is relatively low, leading to a reduced leaching rate of other elements from the steel slag, resulting in a higher Ca content in the material. On the

other hand, when the solid-to-liquid ratio is large, the contact between the acetic acid solution and the steel slag is insufficient, leading to a lower leaching rate of calcium-based components in the converter slag. At a solid-to-liquid ratio of 1:20, the CaO mass fraction increases. This phenomenon is due to the increase in H^+ content, which enables more reactions with the steel slag, raising the solution's pH, which in turn causes the gradual formation of $Fe(OH)_3$ precipitates from the Fe ions in the solution. In conclusion, moderately reducing the solid-to-liquid ratio can effectively enhance the CaO content.

2.2.3 Leaching temperature

As shown in Fig.4c, with the increase in leaching temperature, the CaO mass fraction first decreases and then rises. At a leaching temperature of 70 °C, the CaO content reaches its highest value of 81.3%. When the temperature rises from 30 °C to 40 °C, the CaO content decreases due to the leaching of silicon from the steel slag, forming silica gel that adheres to the surface of solid particles, thereby hindering the contact between acetic acid and the solid material. However, as the temperature continues to rise, the CaO content increases because the acetates in the solution convert into precipitates, which adsorb the silica gel, and through stirring, the silica gel adhered to the solid particles can be desorbed. Additionally, increasing the temperature promotes the ionization of acetic acid. The rise in temperature also accelerates the non-uniform movement of H^+ , leading to a faster reaction rate between H^+ and the calcium-containing components in the steel slag, thus enhancing the leaching rate of Ca^{2+} . In conclusion, higher leaching temperatures can effectively increase the CaO content in calcium-based materials.

2.2.4 Leaching time

As shown in Fig.4d, equilibrium is reached within a 0.5 to 1 h leaching time for steel slag of different particle sizes. This phenomenon is because extending the time by an additional 0.5 h does not result in a significant change in the H^+ content of the solution. As time progresses, the amorphous Si in the steel slag dissolves into the leaching solution in SiO_3^{2-} , causing the silicon concentration to rise gradually and decreasing the CaO mass fraction. However, with further increases in leaching time, the SiO_3^{2-} in the solution gradually combines with free H^+ to form silicic acid (H_2SiO_3), which further hydrates to form orthosilicic acid (H_4SiO_4). The orthosilicic acid molecules then cross-link and condense into silica gel, eventually precipitating out, thereby reducing the concentration of Si while increasing the CaO mass fraction. In conclusion, appropriately extending the leaching time can effectively reduce the Si content in the leachate, thus enhancing the CaO content. Considering time efficiency, the optimal leaching time is 2 h.

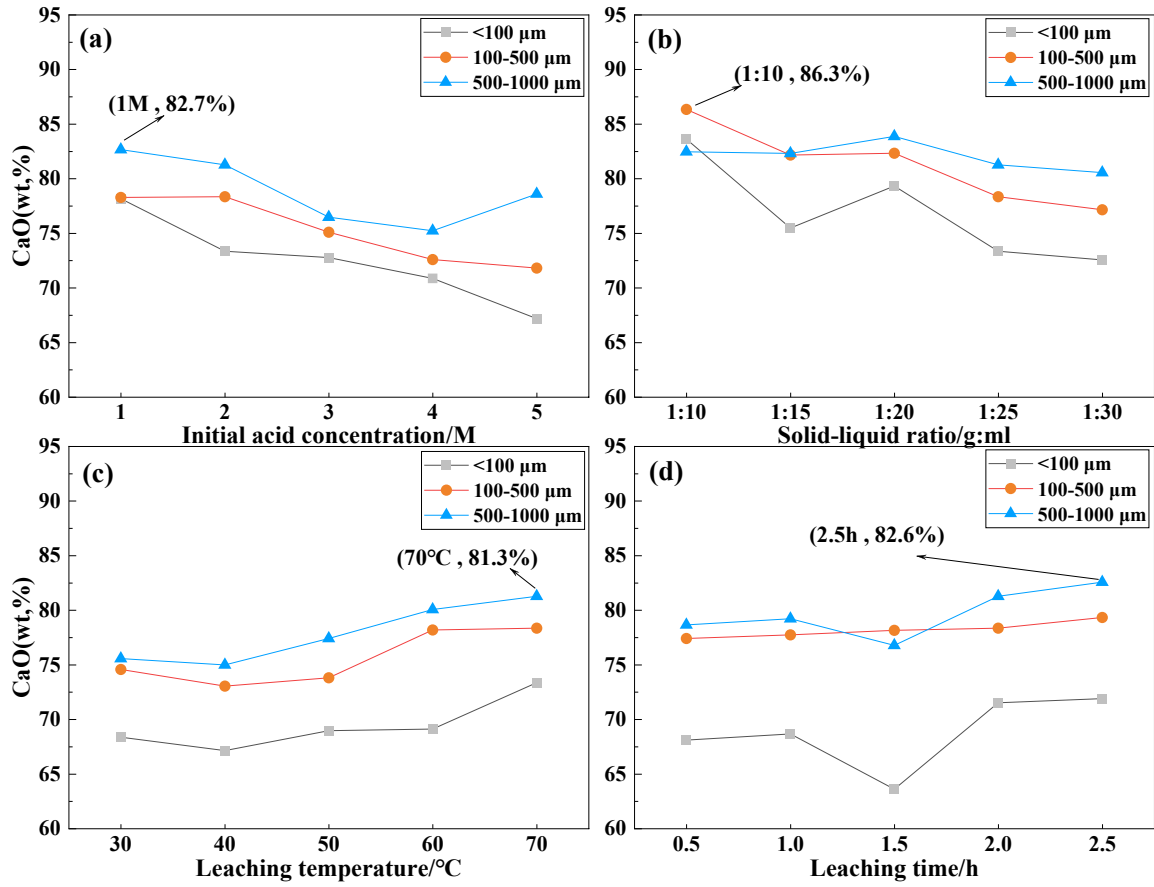


Fig.4 Effect of leaching parameters on CaO content (a)Initial acid concentration (b)Solid-liquid ratio (c)leaching temperature (d)leaching time

2.3 Leaching Kinetics Analysis

2.3.1 Leaching Kinetics Model

The leaching reaction of Ca in steel slag belongs to a solid-liquid heterogeneous reaction. The shrinking core model (SCM) is commonly employed for the kinetic analysis of leaching in such reactions. According to the SCM, the dissolution process involves the following steps [18]:

- (1) The movement of the solvent toward the surface of the solid particles.
- (2) The solvent diffusion from the surface of the solid reaction product to the product-raw material interface.
- (3) Chemical reaction.
- (4) The diffusion of the reaction product from the product layer to the particle surface.
- (5) The outward diffusion of the reaction product from the particle surface to the surrounding area.

According to the SCM, the leaching process has three rate-controlling steps: external diffusion, chemical reaction, and internal diffusion. The specific kinetic equations are presented in Table 2. Here, R represents the element leaching rate; k denotes the rate constant, and t is the leaching time.

Table 2 The relationships of the shrinking core model for a sphere particle [19]

Controlling step	Kinetic equation	Serial number
outward diffusion	$R=kt$	(5)
Chemical reaction	$1-(1-R)^{1/3}=kt$	(6)
inward diffusion	$1-3(1-R)^{2/3}+2(1-R)=kt$	(7)

2.3.2 Kinetic analysis under different stirring rates

The leaching rates of Ca^{2+} at different stirring rates (0, 100, 200, and 400 rpm) were calculated. As seen in Fig.5, the Ca^{2+} leaching rate increases almost consistently at intervals when the stirring rate rises from 0 to 200 rpm. However, when the stirring rate increases to 400 rpm, there is no significant change in the Ca^{2+} leaching rate. This phenomenon indicates that further increasing the stirring rate has little effect on the leaching rate. The Ca^{2+} leaching curve without stirring was further linearized using equations (5), (6), and (7). Within the 0 to 150 min range, the R^2 values are 0.9832, 0.9842, and 0.9246, with 0.9832 and 0.9842 being closest to 1, indicating that the calcium leaching process without stirring is controlled by external diffusion and surface chemical reaction.

Nevertheless, the rate-determining steps of the calcium leaching process vary at agitation rates of 100 rpm, 200 rpm, and 400 rpm. At stirring rates of 100 rpm, 200 rpm, and 400 rpm, the R^2 values obtained from equation (7) are 0.9277, 0.9338, and 0.9028, respectively, with the closest values to 1. Thus, at stirring rates of 100, 200, and 400 rpm, the calcium leaching process is controlled by internal diffusion. It can be inferred that, under stirring conditions, the calcium leaching process is hindered by the formation of insoluble products coating the surfaces of the particles. Therefore, increasing the stirring rate can effectively enhance the contact efficiency between the solvent and the steel slag particles, thereby improving the reaction rate [20].

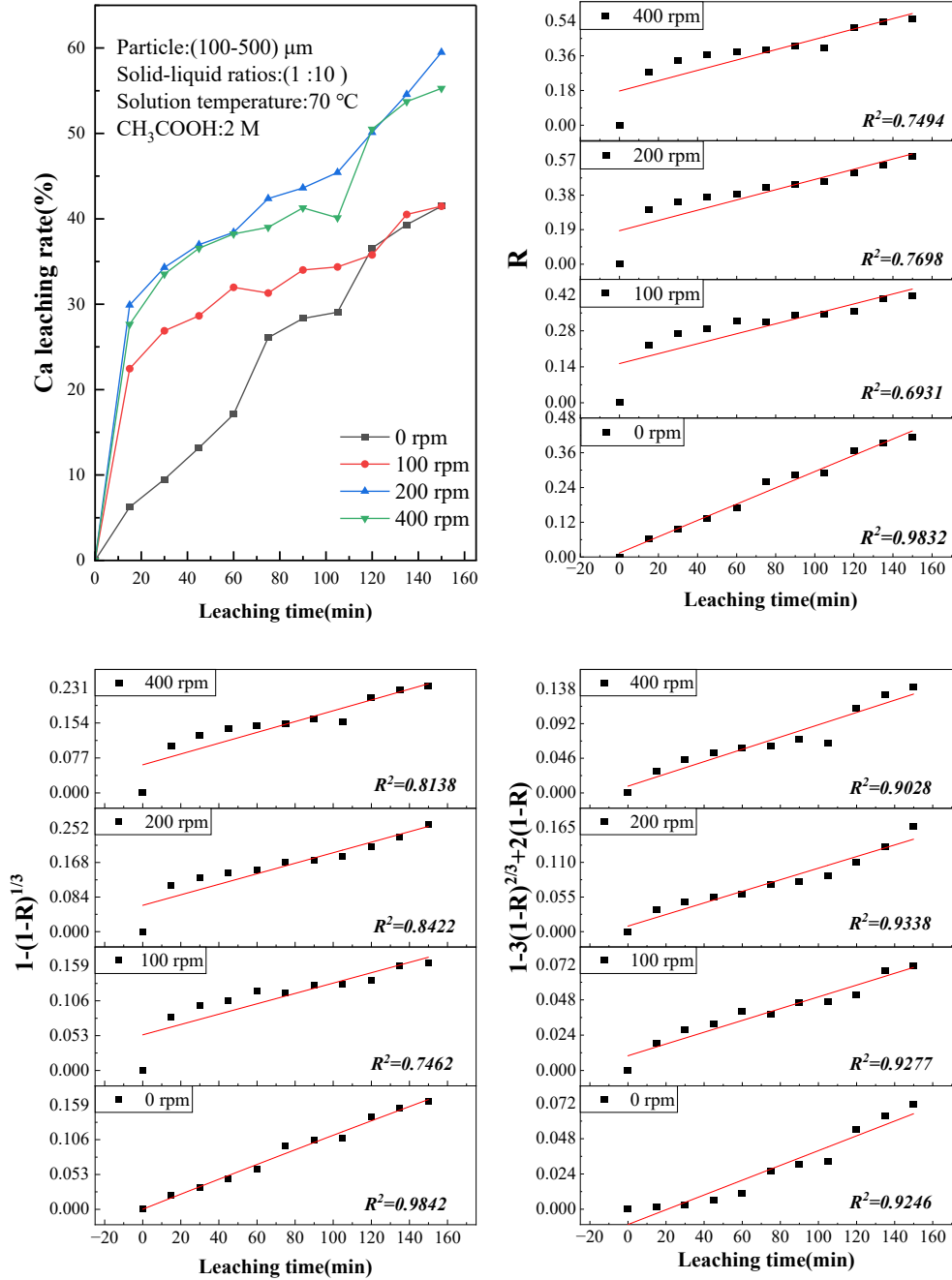


Fig.5 Leaching kinetics model applied to Ca leaching at different stirring speeds

2.3.3 Kinetic analysis at different temperatures

The leaching rates of Ca^{2+} were calculated at temperatures of 40, 50, 60, and 70 $^{\circ}\text{C}$. As shown in Fig.6, the Ca^{2+} leaching rate exhibits only minor differences and a downward trend between 0 and 100 min when the temperature increases from 40 $^{\circ}\text{C}$ to 50 $^{\circ}\text{C}$. However, after 100 min, the leaching rate gradually increases with rising temperature. This phenomenon indicates that as the temperature rises from 40 $^{\circ}\text{C}$ to 50 $^{\circ}\text{C}$, the influence of temperature on the Ca^{2+} leaching rate becomes more pronounced after a certain reaction period. The observed decrease may be attributed to the thermodynamic perspective that the dissolution reaction of lime (CaO) is exothermic, suggesting that the leaching rate should decrease with increasing temperature. When the temperature is maintained at 60 $^{\circ}\text{C}$ and 70 $^{\circ}\text{C}$, the Ca^{2+} leaching rate significantly improves. This enhancement is likely due to the elevated solution temperature, which facilitates the diffusion of molecules in the aqueous phase.

By linearizing the Ca^{2+} leaching curves using equations (5), (6), and (7) (see Fig.6), it is evident that within the temperature range of 40 to 70 °C, equation (7) yields the highest R^2 values, which are 0.7491, 0.9428, 0.9479, and 0.9422, respectively. Therefore, in the range of 40 to 70 °C, the rate-controlling steps of the calcium leaching process remain unchanged and are still governed by internal diffusion, possibly influenced by the mass transfer processes within the surface products covering the particles. Consequently, facilitating the diffusion of Ca^{2+} in the region of the slag particles is crucial for enhancing the leaching rate. In summary, increasing the solution temperature can effectively promote the diffusion of Ca^{2+} , thereby improving the reaction rate.

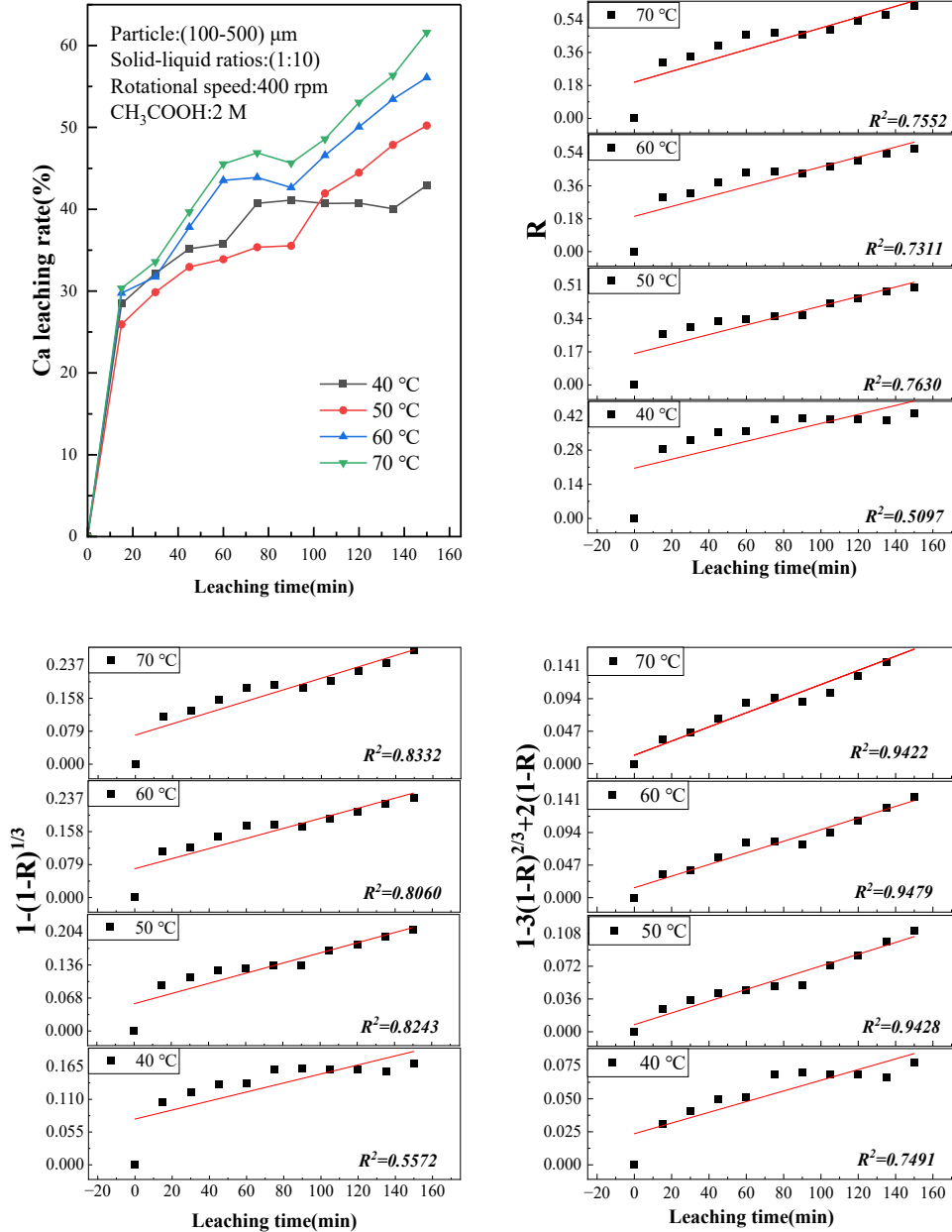


Fig.6 Leaching kinetics model applied to Ca leaching at different leaching temperatures

2.4 XRD and SEM analysis of CaO materials

XRD analysis was conducted on materials prepared under different leaching parameters (selecting three variables). As shown in Fig.7, the phase composition of the materials consists primarily of CaO with a small amount of Fe_2O_3 , indicating a high purity of CaO. Correlating with the variation of CaO mass fraction with various parameters discussed in Section 2.2, it is evident that the intensity of

the CaO diffraction peaks also changes accordingly, following the same trend. This phenomenon suggests that a low concentration of acetic acid solution and a lower solid-to-liquid ratio can significantly enhance the CaO content, while the leaching time does not significantly affect the CaO content. Fig.7(d) and (e) present the microstructure of the CaO materials, revealing two distinct crystal structures (A and B). Energy dispersive spectroscopy (EDS) analysis of A and B shows that their primary elemental compositions are Ca and O. Combining the phase analysis results, both crystal structures represent CaO. This comprehensive analysis further confirms that the prepared materials are of high-purity CaO.

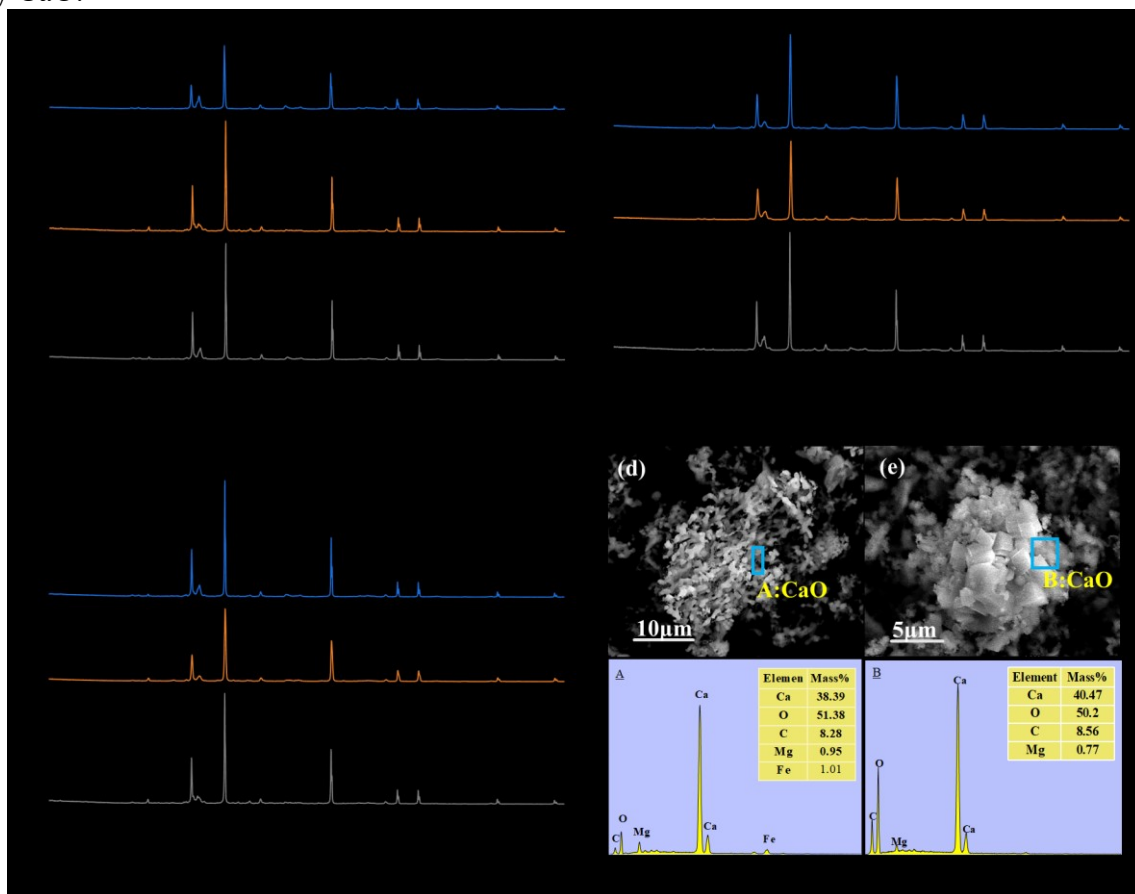


Fig.7 XRD and SEM images of CaO materials prepared under various leaching circumstances (a)Initial acid concentration (b)Solid-liquid ratio (c)leaching time (d,e)SEM

2.5 Effect of CaO content on the CO₂ adsorption performance of the materials

2.5.1 Adsorption performance

Three samples prepared at different leaching temperatures were selected and labelled W1-W3, with their CaO contents increasing sequentially (see Fig.8(d)). During the desorption process, W1-W3 exhibited endothermic peaks at various temperature ranges and showed two main weight loss intervals. First, within the temperature range of 400-450 °C, the curves displayed pronounced endothermic peaks, indicating that the system was in an endothermic state. This phenomenon is primarily attributed to chemically adsorbed water and crystallization water desorption, with the highest weight loss rate occurring at the corresponding peak temperature. As the decomposition temperature increased, the weight loss gradually slowed down. Around 590 °C, weight loss increased alongside the emergence of partial endothermic peaks, and at approximately 750 °C, the weight loss began to stabilize. This stage corresponds to the decomposition reaction of CaCO₃, which releases CO₂. Calculations revealed that the CO₂ capture capacities for W1-W3 were approximately 0.064 g/g, 0.145 g/g, and 0.091 g/g, respectively (see Fig.8(d)). The results indicate that W2 has the highest CO₂ capture capacity, suggesting that a higher CaO content can enhance CO₂ adsorption effectiveness; however,

an excessive CaO content may inhibit the adsorption process.

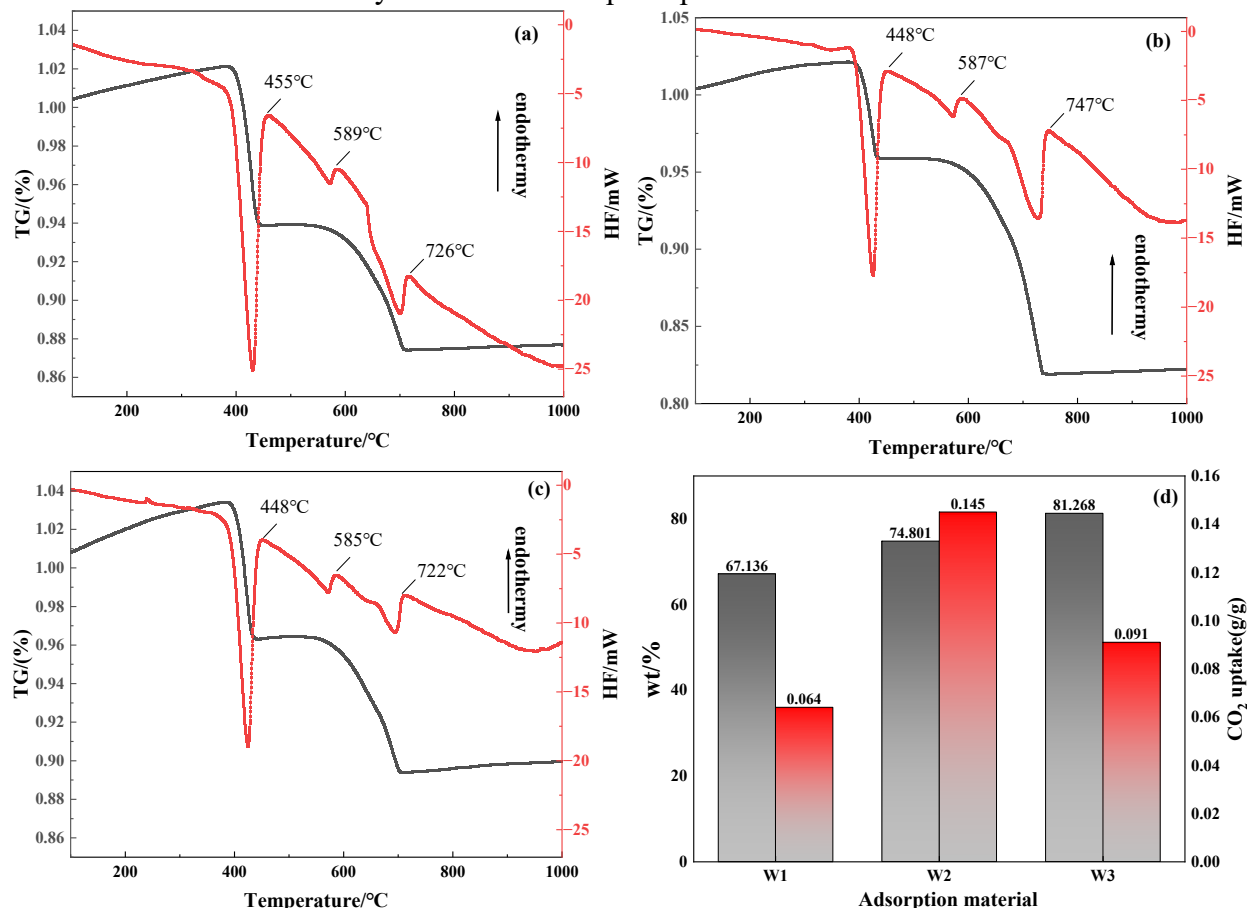


Fig.8 Temperature desorption curve of W1-W3 (a)W1 (b)W2(c)W3

2.5.2 XRD analysis of the materials before and after CO₂ adsorption

Based on the trend of increasing CaO content shown in Fig.8d, the structures of W1-W3 were characterized (see Fig.9a). The primary phase of W1-W3 is CaO, along with a small amount of Fe₂O₃. Furthermore, as the CaO content increases, the intensity of the diffraction peaks also gradually rises. Subsequently, after W1-W3 adsorbed CO₂, an additional XRD analysis was performed, and the results are presented in Fig.8b. When the CaO content is low, the phase composition consists of Ca(OH)₂ and CaCO₃ (see Fig.9b-W1). Due to the low CaO content in the material, the surface-active CaO is insufficient to adsorb all the CO₂ and form CaCO₃, resulting in a significant amount of Ca(OH)₂ remaining after CO₂ adsorption for some time.

As the CaO content increases, the phase completely transforms into CaCO₃ (see Fig.9b-W2). This phenomenon occurs because the higher CaO content leads to increased formation of Ca(OH)₂, and the rate of Ca(OH)₂ formation is consistent with the rate at which Ca(OH)₂ adsorbs CO₂. Consequently, the phase composition remains unchanged, and at the end of the adsorption process, only CaCO₃ is present. This phenomenon indicates that an increase in CaO content facilitates the absorption of more CO₂ and yields pure carbonate.

As the CaO content further increases, the intensity of the CaCO₃ phase diffraction peaks does not show significant enhancement, and the Ca(OH)₂ phase reappears (see Fig.9b-W2). This phenomenon indicates that, with the increase in CaO content and the subsequent adsorption of more CO₂, the amount of CaCO₃ increases and adheres to the material surface. This adhesion hinders the contact and reaction between Ca(OH)₂ and CO₂, reducing carbonation efficiency [21].

Therefore, moderately increasing the CaO content can enhance CO₂ adsorption performance, but excessive CaO does not necessarily significantly improve adsorption capacity. It is also essential

to optimize other adsorption conditions during the process to achieve the maximum CO₂ capture efficiency.

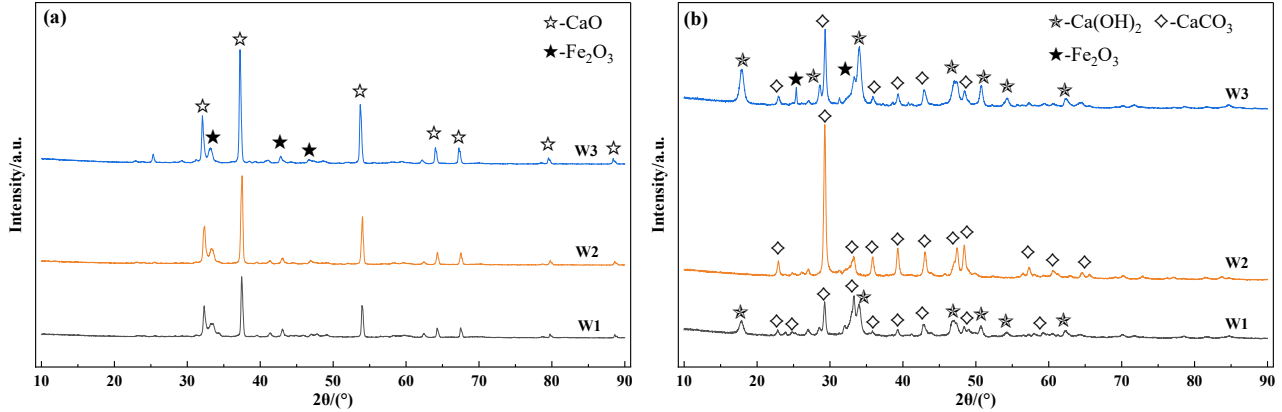


Fig.9 Desorption curves of calcium-based materials W1-W3 at temperature
(a) Pre-adsorption (b) Post-adsorption

2.5.3 SEM analysis of the materials before and after CO₂ adsorption

By conducting SEM analysis before and after the adsorption process, we can better understand the adsorption mechanism and validate the effect of CaO content on adsorption performance. SEM analysis was performed on W1-W3 after CO₂ adsorption; the results are shown in Fig.10. Fig.10(b), (d), and (e) display the microstructures of W1-W3 after CO₂ adsorption. Two distinct color regions can be observed on the surface, such as A1 and A2, in Fig.10(b). BSE analysis (Fig.10(c,f)) reveals that the bright white regions correspond to CaCO₃, while the darker regions represent Ca(OH)₂. Furthermore, the EDS analysis of Fig.10(d) indicates that this material is primarily CaCO₃ with high purity (Fig.10(j-m)). This phenomenon suggests that during adsorption, CaO on the material surface first adsorbs water vapor to form Ca(OH)₂, which then adsorbs CO₂, forming CaCO₃ that adheres to the material surface.

Additionally, it can be observed that as the CaO content increases (from Fig.10(b) to 10(d)), the bright white regions expand, indicating an increase in CaCO₃ content. However, as the CaO content continues to rise (from Fig.10(d) to 10(e)), the CaCO₃ formed on the surface can hinder the reaction between Ca(OH)₂ and CO₂, leading to a reduction in reaction rate. Similarly, the quantity of Ca(OH)₂ influences the purity of CaCO₃. In conclusion, a moderate increase in CaO content can enhance CO₂ adsorption performance.

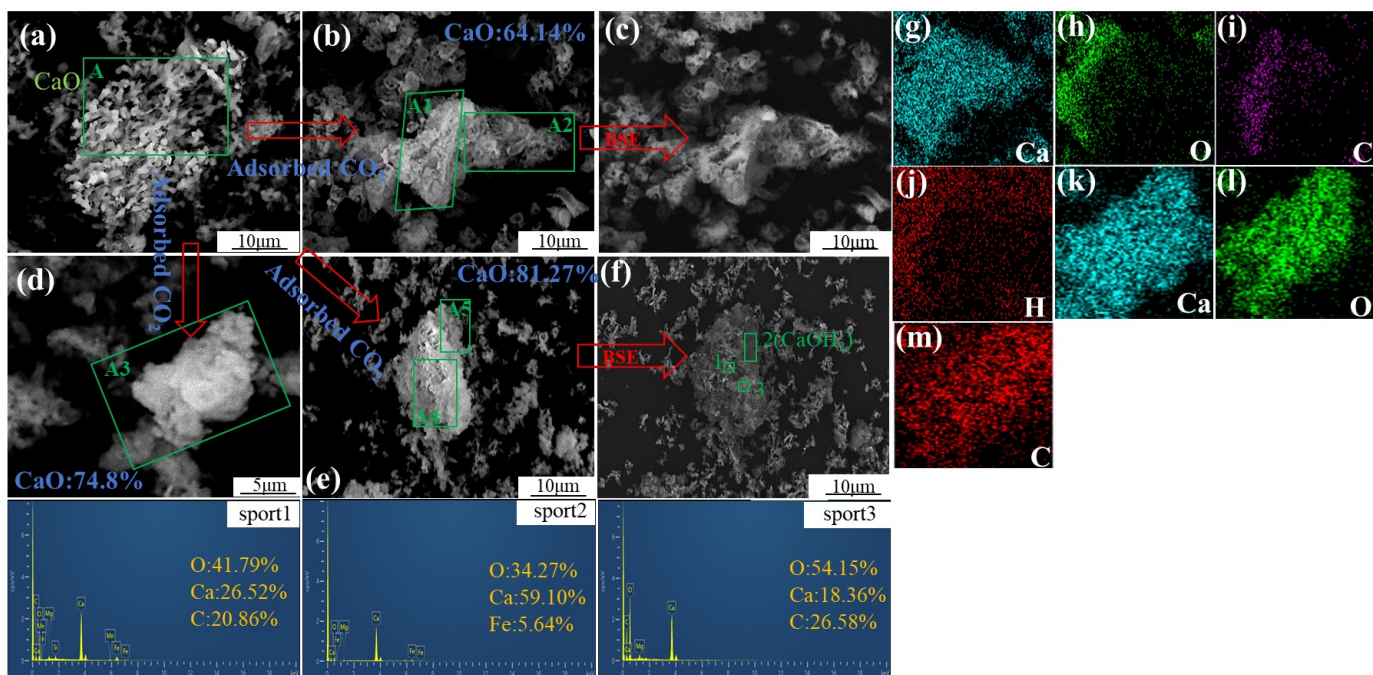


Fig.10 Morphology, structure, and energy spectrum analysis of BSE after CO₂ adsorption by W1-W3(a) Original material (b)W1 (d)W2 (e)W3

2.6 Effect of adsorption temperature on the CO₂ adsorption performance of the materials

The adsorption performance of the materials was tested at adsorption temperatures of 30 °C, 50 °C, and 70 °C, with the resulting temperature-programmed desorption curves shown in Fig.11. Each thermal flow curve exhibits two endothermic intervals corresponding to a specific weight loss process, as the TG curve reflects. In the 400-450 °C range, the primary processes involve the desorption of chemically adsorbed water and crystallization water, with the weight loss rate peaking at the corresponding temperature. In the 600-800 °C range, the primary reaction is the decomposition of CaCO₃, which releases CO₂.

At temperatures of 30 °C, 50 °C, and 70 °C, the mass changes were 34.3%, 24.6%, and 19.1%, respectively. Calculations revealed the CO₂ capture capacities to be 0.32 g/g, 0.24 g/g, and 0.17 g/g, with corresponding carbon fixation efficiencies of 47.39%, 34.89%, and 25.65% (see Fig.11(c)). Thus, carbon fixation efficiency decreases within the 0-100 °C range as the temperature rises. This phenomenon may be attributed to two primary reasons: firstly, analysis of the ΔG for the reactions between CaO and Ca(OH)₂ with CO₂ indicates that as temperature increases, ΔG also rises, suggesting a reduction in the spontaneity of the reaction (see Fig.11(b)). Secondly, as the temperature rises, more CaCO₃ adheres to the material surface, hindering the contact between CO₂ and Ca(OH)₂, reducing CO₂ capture capacity. In summary, within the adsorption temperature range of 0-100 °C, there is an inverse relationship between temperature and CO₂ capture capacity.

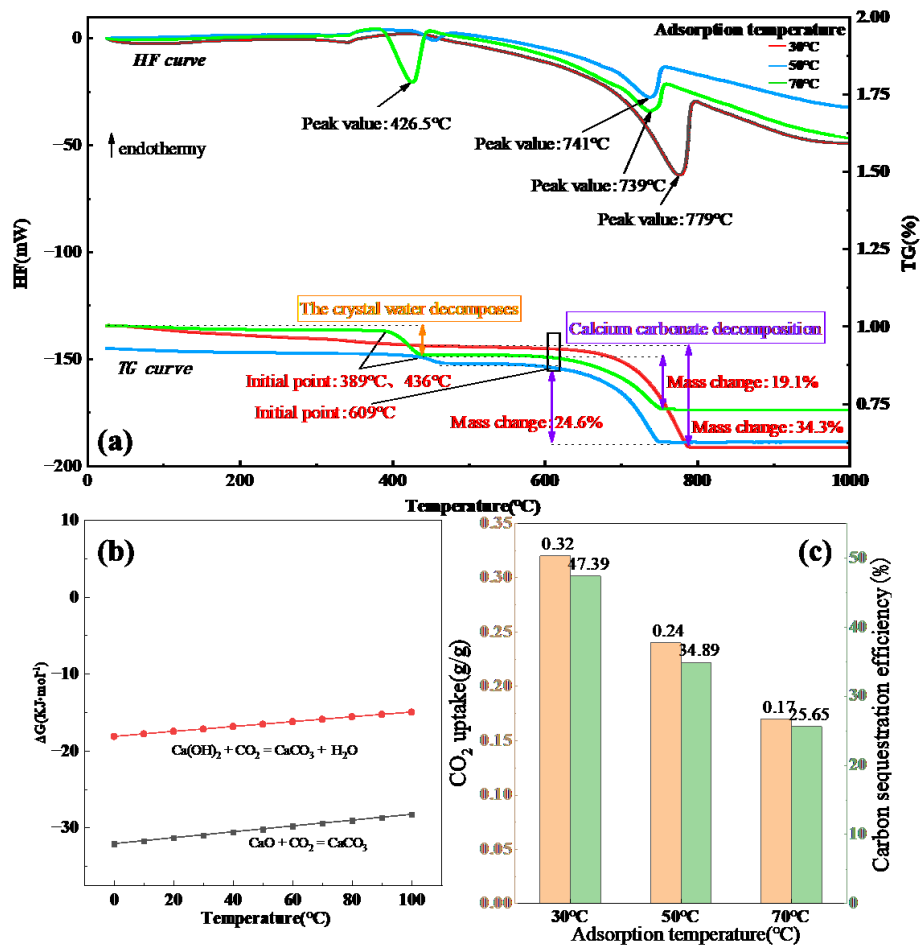


Fig.11 CO₂ adsorption properties of adsorbed materials at different adsorption temperatures

XRD analysis was conducted to investigate further the impact of adsorption temperature on the material's capacity to adsorb CO₂ (Fig.12). At 30 °C, upon completion of adsorption, the diffraction peaks corresponding to CaO nearly disappeared, ultimately transforming into the CaCO₃ phase. At 50 °C, the diffraction peaks of CaO diminished, with some even vanishing, resulting in a small amount of Ca(OH)₂ and a significant presence of CaCO₃. By the end of the adsorption process at 70 °C, the diffraction peak for Ca(OH)₂ was notably enhanced. This thermal progression's influence on the phases can be elucidated as follows: at 30 °C, CaO, upon adsorbing water vapor, entirely converted into Ca(OH)₂, while Ca(OH)₂ adsorbing CO₂ fully transformed into CaCO₃, reaching an equilibrium in the rates of these transformations. As the temperature increased to 50 °C, the conversion rate of CaCO₃ accelerated, impeding some Ca(OH)₂ from interacting with CO₂. At 70 °C, the diffraction peak for Ca(OH)₂ markedly intensified, indicating that an increased amount of Ca(OH)₂ could not engage with CO₂, reducing the reaction rate.

Consequently, elevated temperatures lead to a greater formation of CaCO₃, which obstructs the carbonation reaction. Within the adsorption temperature range of 0-100 °C, ensuring that more Ca(OH)₂ effectively interacts with CO₂ is crucial. At lower adsorption temperatures, the material's adsorption performance significantly improves.

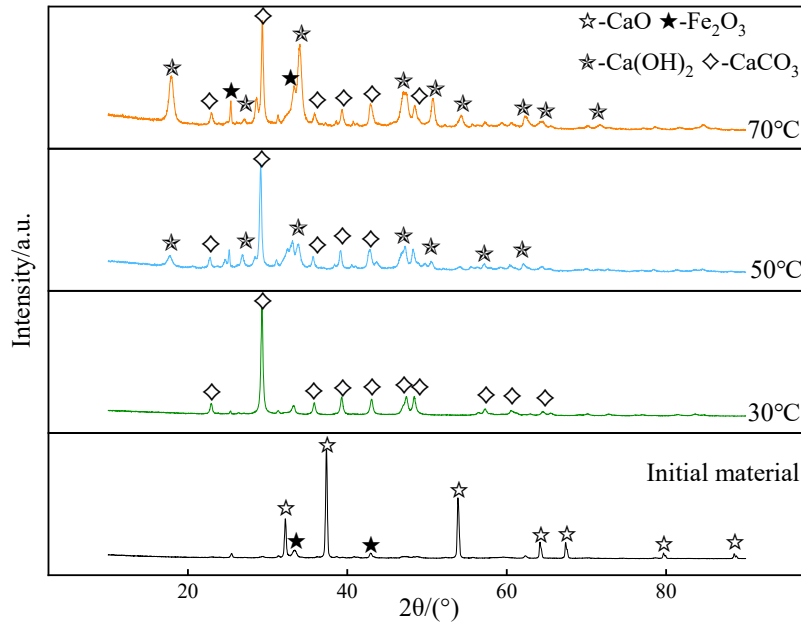


Fig.12 XRD pattern of the initial material and CO₂ adsorbed at different adsorption temperatures

3. Conclusion

(1) The leaching temperature and acetic acid concentration significantly influence the CaO content in the material. The optimal leaching parameters are an acid concentration of 1 M, a solid-to-liquid ratio of 1:10 (g: ml), a leaching temperature of 70 °C, and a duration of 2 h, under which the CaO content reaches a maximum of 86.3%. This phenomenon indicates that a low concentration of acid combined with a higher temperature can effectively enhance the mass fraction of CaO in the material.

(2) In the absence of stirring, the process is controlled by external diffusion and surface chemical reactions. Under stirring conditions, internal diffusion governs the calcium leaching process. It can be inferred that, under stirring conditions, the leaching process is hindered by the de. position of insoluble products on the surface of the particles. Within the temperature range of 40-70 °C, internal diffusion becomes the rate-controlling step, likely due to mass transfer limitations in the products covering the particle surfaces. Therefore, increasing the stirring rate can effectively enhance the contact efficiency between the solvent and the steel slag particles while elevating the solution temperature can significantly promote the diffusion of Ca²⁺, thereby increasing the CaO content.

(3) The adsorption process unfolds as follows: CaO in the material reacts with water vapor to form Ca(OH)₂, with the concentration of CaO determining the resulting amount of Ca(OH)₂. Subsequently, Ca(OH)₂ adsorbs CO₂, leading to the formation of CaCO₃. This CaCO₃ adheres to the material's surface, obstructing the interaction and reaction between Ca(OH)₂ and CO₂, thereby diminishing the carbonation efficiency.

(4) A moderate increase in CaO content can significantly enhance CO₂ adsorption performance; however, this does not imply that excessive CaO will yield further improvements. Calculations indicate that the CO₂ adsorption capacity of W2 can reach 0.145 g/g. Within the adsorption temperature range of 0-100 °C, ensuring that more Ca(OH)₂ effectively interacts with CO₂ is crucial. The material's adsorption performance is markedly improved at lower adsorption temperatures, with CO₂ capture amounts recorded at 30 °C, 50 °C, and 70 °C being 0.32 g/g, 0.24 g/g, and 0.17 g/g, respectively.

Acknowledgments:

None.

Author's contributions:

Jie Cheng: Research methods, data sorting, and manuscript writing

Rui Mao: Revise, comment

Fei Wang and Haiwei Yao: validation, writing-reviewing and editing.

All authors read and approved the final version of the manuscript.

Data availability:

The data that support the findings of this study are available on request from the First author

Conflict of interest:

There is no conflict of interest.

Reference

- [1] T.S. Naidu, C.M. Sheridan, L.D. van Dyk, Basic oxygen furnace slag: Review of current and potential uses, *Minerals Engineering*, 149 (2020) 355-365. <https://doi.org/10.1016/j.mineng.2020.106234>
- [2] W. Gao, W. Zhou, X. Lyu, X. Liu, H. Su, C. Li, H. Wang, Comprehensive utilization of steel slag: A review, *Powder Technology*, 422 (2023) 2308-2341. <https://doi.org/10.1016/j.powtec.2023.118449>
- [3] R. Chen, G.X. Wu, L.L. Li, Z.L. Zhang, Y. Sun, X.L. Li, Y. Liu, Y. Huang, Z.S. Zou, Carbonation reaction of slag from steel refining for CO₂ sequestration in the absence and presence of water vapor, *Science of Advanced Materials*, 11(5) (2019) 749-755. <https://doi.org/10.1166/sam.2019.3495>
- [4] G. Liu, K. Schollbach, S. van der Laan, P. Tang, M.V.A. Florea, H.J.H. Brouwers, Recycling and utilization of high volume converter steel slag into CO₂ activated mortars—The role of slag particle size. *Resources, Conservation and Recycling*, 160 (2020) 48-83. <https://doi.org/10.1016/j.resconrec.2020.104883>
- [5] R. Ragipani, S. Bhattacharya, A.K. Suresh, A review on steel slag valorization via mineral carbonation, *Reaction Chemistry & Engineering*, 6.7 (2021) 1152-1178. <https://doi.org/10.1039/D1RE00035G>
- [6] D. He, L. Yang, Y. Luo, G. Liu, Z. Wu, Synergistic calcium leaching and iron enrichment by indirect carbonation of thermally modified steel slag, *Construction and Building Materials*, 411 (2024) 342-347. <https://doi.org/10.1016/j.conbuildmat.2023.134249>
- [7] E.E. Chang, S.Y. Pan, Y.H. Chen, H.W. Chu, C.F. Wang, P.C. Chiang, CO₂ sequestration by carbonation of steelmaking slags in an autoclave reactor, *Journal of Hazardous Materials*, 195 (2011) 107-114. <https://doi.org/10.1016/j.jhazmat.2011.08.006>
- [8] H.P. Mattila, R. Zevenhoven, Design of a continuous process setup for precipitated calcium carbonate production from steel converter slag, *ChemSusChem*, 7(3) (2014) 903-913. <https://doi.org/10.1002/cssc.201300516>
- [9] M. Owais, M. Järvinen, P. Taskinen, A. Said, Experimental study on the extraction of calcium, magnesium, vanadium and silicon from steelmaking slags for improved mineral carbonation of CO₂, *Journal of CO₂ Utilization*, 31 (2019) 1-7. <https://doi.org/10.1016/j.jcou.2019.02.014>
- [10] Y. H. Lee, H. Eom, S. M. Lee, S. S. Kim, Effects of pH and metal composition on selective extraction of calcium from steel slag for Ca(OH)₂ production, *RSC advances*, 11(14) (2021) 8306-8313. <https://doi.org/10.1039/D0RA08497B>
- [11] L.L. Li, R. Chen, Z.L. Zhang, Preparation of calcium-based CO₂ adsorption materials by acetic acid leaching of calcium components from refining slag, *Journal of Iron and Steel Research*, 2020, 32(7): 6-9. <https://doi.org/10.13228/j.boyuan.issn1001-0963.20200036>

- [12]D. Fang, L. Zhang, L. Zou, F. Duan, Effect of leaching parameters on the composition of adsorbents derived from steel slag and their CO₂ capture characteristics, *Greenhouse Gases: Science and Technology*, 11(5) (2021) 924-938. <https://doi.org/10.1002/ghg.2103>
- [13]F. Yan, K. Luo, J. Ye, W. Zhang, J. Chen, X. Ren, Z. Liu, J. Li, Leaching kinetics and dissolution model of steel slag in NaOH solution, *Construction and Building Materials*, 434 (2024) 1123-1134. <https://doi.org/10.1016/j.conbuildmat.2024.136743>
- [14]Z. Zhu, X. Gao, S. Ueda, S. Kitamura, Contribution of mineralogical phases on alkaline dissolution behavior of steelmaking slag, *ISIJ International*, 59(10) (2019) 1908-1916. <https://doi.org/10.2355/isijinternational.ISIJINT-2019-049>
- [15]Y. Kashiwaya, S. Tauchi, T. Nomura, T. Akiyama, Kinetic Analysis Considering Particle Size Distribution on Ca Elution from Slags in CaO–SiO₂–MgO–Al₂O₃–Fe₂O₃ System, *ISIJ International*, 60(12) (2020) 2859-2869. <https://doi.org/10.2355/isijinternational.ISIJINT-2020-265>
- [16]R. Ragipani, S. Bhattacharya, A.K. Suresh, Kinetics of steel slag dissolution: from experiments to modelling, *Proceedings of the Royal Society A*, 475.2224 (2019) 523-533. <https://doi.org/10.1098/rspa.2018.0830>
- [17]S. Yokoyama, A. Suzuki, H. B. M. N Nik, H.K. anematsu, A. Ogawa, T. Takahashi, M. Umemoto, Serial batch elution of electric arc furnace oxidizing slag discharged from normal steelmaking process into fresh water, *ISIJ international*, 50(4) (2010) 630-638. <https://doi.org/10.2355/isijinternational.50.630>
- [18] C.F. Tang, R.L. Zhang, W. Zhang, R.X. Yang, C. Li, J. Zeng, Kinetics Study on the Leaching of Copper from Calcification Roasting Copper Refining Slag Using Waste Acid, *Mining, Metallurgy & Exploration*, 40(1) (2023) 171-179. <https://doi.org/10.1007/s42461-022-00727-5>
- [19]K. Hinrichsen, E. Klemm, *Chemical Reaction Engineering, Chemical Engineering & Technology*, Wiley, 2016, 1992-1992.
- [20]E. Kusaka, R. Suehiro, Y. Iwamizu, Kinetics of calcium leaching from particulate steelmaking slag in acetic acid solution, *Isij International*, 62(1) (2022) 263-274. <https://doi.org/10.2355/isijinternational.ISIJINT-2021-121>
- [21]D. He, L. Yang, Y. Luo, G. Liu, Z. Wu, Synergistic calcium leaching and iron enrichment by indirect carbonation of thermally modified steel slag, *Construction and Building Materials*, 411, (2024)114-128. <https://doi.org/10.1016/j.conbuildmat.2023.134249>

Table1	Single-factor experimental parameters of the acetic acid leaching process
Table2	The relationships of the shrinking core model for a sphere particle
Figure1	XRD pattern of the steel slag
Figure2	Schematic Illustration of the Synthetic Procedure for the Preparation of the CaO material from Converter Steel Slag
Figure3	Gibbs free energy of acid hydrolysis reaction of main calcium-base phase in steel slag at different temperatures (atmospheric pressure)
Figure4	Effect of leaching parameters on CaO content (a)Initial acid concentration (b)Solid-liquid ratio (c)leaching temperature (b)leaching time
Figure5	Leaching kinetics model applied to Ca leaching at different stirring speeds
Figure6	Leaching kinetics model applied to Ca leaching at different leaching temperatures
Figure7	XRD and SEM images of CaO materials prepared under various leaching circumstances (a)Initial acid concentration (b)Solid-liquid ratio (c)leaching time (d,e)SEM
Figure8	Temperature desorption curve of W1-W3 (a)W1 (b)W2(c)W3
Figure9	Desorption curves of calcium-based materials W1-W3 at temperature

	(a) Pre-adsorption (b)Post-adsorption
Figure10	Morphology, structure, and energy spectrum analysis of BSE after CO ₂ adsorption by W1-W3(a) Original material (b)W1 (d)W2 (e)W3
Figure11	CO ₂ adsorption properties of adsorbed materials at different adsorption temperatures
Figure12	XRD pattern of the initial material and CO ₂ adsorbed at different adsorption temperatures